Using a single structure for three sensor operations and two actuator operations

G.R. Langereis, W. Olthuis and P. Bergveld

MESA Research Institute, University of Twente, P.O. Box 217, 7500 AE Enschede, The Netherlands
Recieved 9 September 1997, accepted 3 August 1998
Printed in: Sensors and Actuators B, 53/3 (1999), page 197 - 203

Summary

In many process control applications, a set of separate existing sensor structures is placed in the environment of interest and not much attention is being paid to the integration of these structures and even less to the possibility of combining the measurement results obtained from these sensor structures. However, a new trend in chemical sensing is the development of sensor arrays and the use of more than one transduction principle applied to the same selective layer [1].
An integrated sensor structure with the highest level of integration was developed and tested. The structure with a size of one square millimeter can be accessed by only four contacting leads. By scheduling this structure in different modes, several sensing modes are selected for determining electrolyte conductivity, temperature and hydrogen peroxide concentration, where the latter one represents one example of many species that can be determined amperometrically. In addition, two actuator functions using the same single structure were tested as well: the local environment was thermoresistively heated and a local pH gradient was created by the electrolysis of water. The two actuator operations together with the three sensor operations makes the structure an excellent starting point for many local experiments, which will lead to the determination of more environmental parameters than the number of sensors present in the array.

Keywords: Sensor array, sensor integration, conductivity, amperometry, thermoresistivity

1. Introduction

Many sensor designers aim at a single, highly selective structure consisting of a selector part and a transducer part. An alternative approach is the use of an array of, usually more, less-selective simple structures where an intelligent control system is used to determine a set of parameters from a number of experiments carried out using these structures. Figure 1 shows the general structure of such an array-based measurement system. The multi purpose sensor-actuator structure described here is an integration of a number of sensor and actuator structures, and can therefore replace a row of separate structures. In terms of figure 1: the

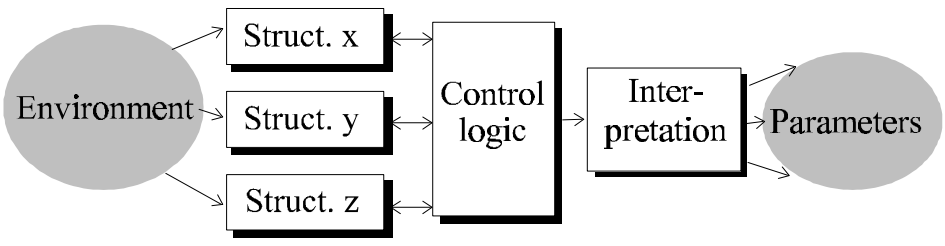

Figure 1: General structure of a sensor array based measurement system.

multi purpose sensor-actuator structure can be used as either structure x, y or z when suitably scheduled by the control logic.
An advantage of performing several measurements using a single structure is that the information certainly comes from the same location in the sample solution. Besides that, the number of contact leads is reduced and the size of the single multi purpose structure will be smaller than the separate structures.

The used structure, as shown in the artist impression of figure 2 and on the photograph of figure 3, consists only of shaped platinum films on a substrate. Its shape is based on an interdigitated structure which is a common design for conductivity sensors [2]. In order to create a resistive path for temperature measurements and heating, the fingers were cut along. With all of the pads in parallel, the structure is a working electrode for amperometric measurements and electrolysis purposes. Notice that for the latter mode of operation an external counter electrode is necessary, which however, can also be integrated with the present device, for instance on the backside.

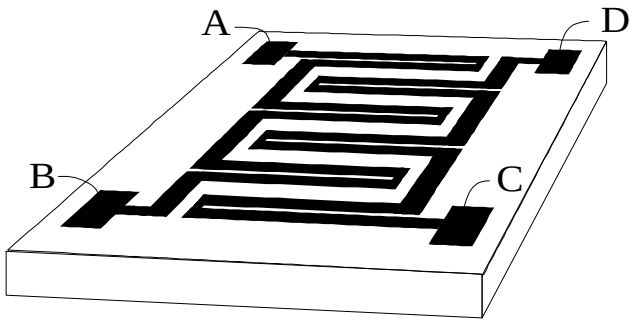

Figure 2: Artist impression of the multi purpose sensor structure. Temperature between pad A and B, Conductivity between pads A, B and C, D, Amperometric working electrode with pads A, B, C, and D short circuited.

Figure 3: Photographs of realised sensor structures: just after sawing (left) and after packaging on a printed circuit board (right)

Two implementations of the structure were realised and tested, differing in the number and width of the fingers. They will be referred to as type I and II. Table 1 gives the dimensions for the two implementations of the sensor-actuator structure.

Table 1: Device dimensions for the integrated sensor structures

	Type I		**Type II**	
	Theory	Measured	Theory	Measured
Conductivity				
Space between fingers [µm]	5		15	
Width of the fingers [µm]	200		100	
Length of the fingers [µm]	1025		1035	
Number of fingers	5		9	
Cell constant [cm^{-1}]	1.65	1.35	1.24	1.28
Temperature				
Length of the resistive path [mm]	10.25		8.28	
Width of the resistive path [µm]	47		45	
Nominal resistance at 20 °C [Ω]	92	69.8	78	63.8
Working electrode [mm^2]	2×0.48		2×0.42	
Size of structure [mm^2]	1.0×1.0		1.0×1.0	

2. Theory

The three basic operational sensing modes of the structure (temperature, conductivity and amperometry) and the two operational actuator modes (local heating and pH gradient control) are selected by choosing the proper connecting pads and applying a specific stimulus to these pads. The parameter to be measured then follows from the voltage-current relation.

2.1 Temperature

The structure of figure 2 has two resistive paths: between pads A and B and between pads C and D. The change in resistance due to temperature variations can be written as:

$$R(T) = R_{Ref} \cdot \left[1 + \alpha\left(T - T_{Ref}\right)\right] \qquad (1)$$

with α the temperature coefficient, T the temperature of the metal, T_{Ref} a reference temperature and R_{Ref} the nominal resistance being theoretically equal to 92 Ω and 78 Ω for sensor type I and II respectively. The temperature coefficient α is found in literature [3] to be 3.92×10^{-3} $°C^{-1}$ for the bulk of platinum with a non-linearity of 0.2% between 0-100 °C.

2.2 Conductivity

When inputs A, B and C, D are short circuited, the structure can be used as an interdigitated structure for electrolyte conductivity measurements [2]. Figure 4 shows the equivalent circuit for a two-points conductivity cell.

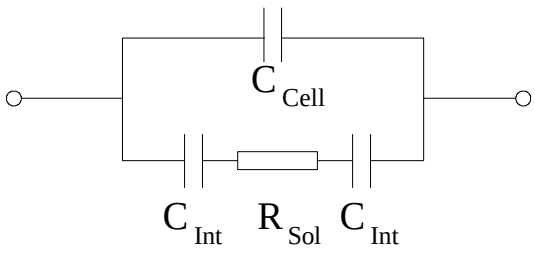

Figure 4: Equivalent circuit for a conductivity cell.

The capacitances C_{Int} represent the metal-electrolyte double layer. Together with the electrolyte resistance R_{Sol} they cause the first cut-off frequency. Above this frequency, the impedance of the structure is practically equal to the electrolyte resistance. From the electrolyte resistance the conductivity k_{Sol} can be found using the geometric constant K_{Cell}:

$$\kappa_{Sol} = \frac{K_{Cell}}{R_{Sol}} \quad (2)$$

The upper limit of the measurement frequency is determined by the cell capacitance C_{Cell} or in some cases by the connecting wires parasitic capacitance which is in parallel to C_{Cell}. The structure was optimised for making the low cut-off frequency as low as possible in order to have a large operational frequency range. The cell constant can be calculated from the dimensions of the structure [2] and is 1.65 cm^{-1} for structure I and 1.24 cm^{-1} for structure II.

2.3 Chrono amperometric operation

As a test system for the amperometric operation of the structure, the oxidation of hydrogen peroxide is taken.

$$H_2O_2 \rightarrow O_2 + 2H^+ + 2e^- \quad (3)$$

The simplicity of the integrated sensor-actuator structure would be completely cancelled when the amperometric measurement was done using a three electrode set-up with a glass reference electrode. Therefore a two electrode technique is used. A voltage ramp is applied to the working electrode with respect to a 0.5´1.0 cm^2 platinum counter electrode while the current is monitored. This current, which is one branch of a cyclic voltammogram in principle [4], shows a dominant peak due to the oxidation of hydrogen peroxide. The peak value is proportional to the hydrogen peroxide concentration. Since the counter electrode is much larger than the working electrode, the observed current behaviour comes mainly from transport and chemical phenomena occurring at the working electrode. In addition, the low current density through the counter electrode ensures that the counter electrode interface potential can be considered to be constant during a measurement.
Although an amperometric determination can be performed using the two available meander shaped structures, a large external counter electrode was used for reasons stated above, and since it was available anyway for the actuator operation. In addition, it gives a better spatial separation avoiding interferences between the electrode reactions.

2.4 Heating

The quantity of heat produced by a thermoresistive heater is equal to:

$$\Delta Q = P \cdot t = I^2 Rt \quad (4)$$

with R the electrical resistance of the heater, t the time and I the electric current. Without determining an explicit temperature/current relation for the system of a heater on a glass substrate in water, it can be proven [5] that the change in temperature is always proportional to the dissipated heat DQ and so to the square of the applied current.

2.5 Local pH gradient control

By applying a current to all four pads of the structure with respect to a counter electrode as described in section 0, two types of the electrolysis of water can be selected:

$$2H_2O \rightarrow O_2 + 4H^+ + 4e^- \quad (5a)$$

$$2H_2O + 2e^- \rightarrow 2OH^- + H_2 \quad (5b)$$

where the first one decreases and the second one increases the local pH. A method for showing this operation for equation 5b, is a coulometric acid to base titration with the electrochemically produced OH^- as base [6]. The measured electrode potential can be used as an end-point indicator because equation 5b shows a pH dependent term according to the Nernst equation:

$$E = E^0 - 0.059 \cdot pH\,. \qquad (6)$$

For such a potentiometric titration of an acid HA, the end point is determined by the Sand equation [4]:

$$t_{end} = \left[\frac{C_{HA,bulk} F \sqrt{\pi D_{HA}}}{2 j_c} \right]^2 \qquad (7)$$

with $C_{HA,bulk}$ the acid bulk concentration, F Faraday's constant, D_{HA} the diffusion coefficient of the acid and j_c the actuator current density.

3. The fabrication process

The platinum structure was realised on a Hoya® glass substrate. For electrical insulation of the inactive parts from the solution, a polyimide mask was used. Tantalum layers were used in order to obtain good adhesion between the platinum layer and glass and between platinum and polyimide. A cross sectional view of the structure is given in figure 5. The devices were mounted on a printed circuit board and packaged with Hysol® resin.

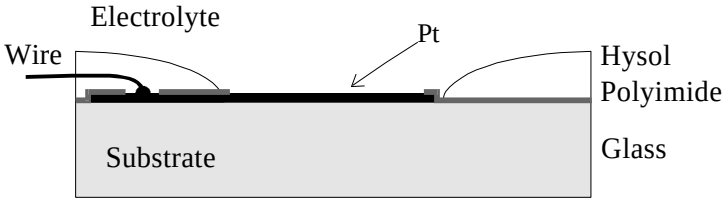

Figure 5: Cross section of the structure.

4. Experimental

The operational modes were tested sequentially by using advanced laboratory equipment (potentiostat, gain-phase analyser). The development of special control electronics for the optimised use of the structure was left for future work.

4.1 Temperature

Between pads A and B of the sensor-actuator structure a dry resistance of 69.8 Ω or 63.8 Ω was found for devices I and II respectively. This value is not completely in agreement with the theoretical values, but this is not a practical problem because the temperature information is in the variations of the nominal resistance.

An automated set-up was used based on a Radiometer CDM210 conductivity meter in resistance measuring mode. This resulted in a

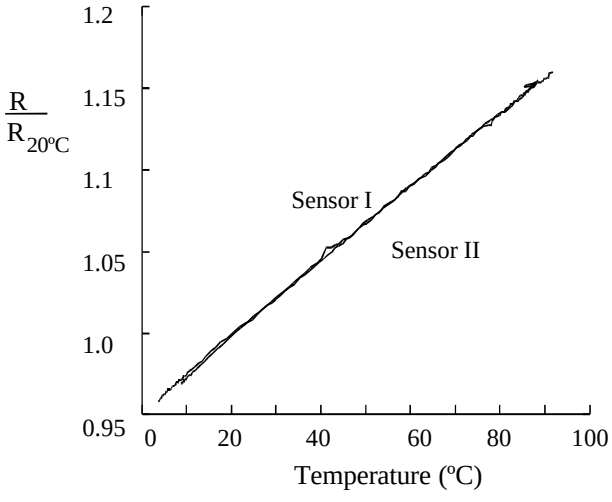

Figure 6: Measured calibration curve for temperature sensing operation.

convenient system for reproducibly recording temperature and resistance. The resistance was measured while heating water, starting with melting ice. The normalised temperature scans for devices I and II are in figure 6. A temperature coefficient of $2.33 \cdot 10^{-3}$ $°C^{-1}$ was found for both types. This value is lower than the one found in literature. This difference, which is probably due to the thin film implementation, was observed already by others [3].

4.2 Conductivity

The impedance plots of the sensors at various KNO_3 concentrations were determined using a HP4194a gain-phase analyser. The two cut-off frequencies behaviour as predicted in the theory is confirmed by the measurement results presented in figure 7.

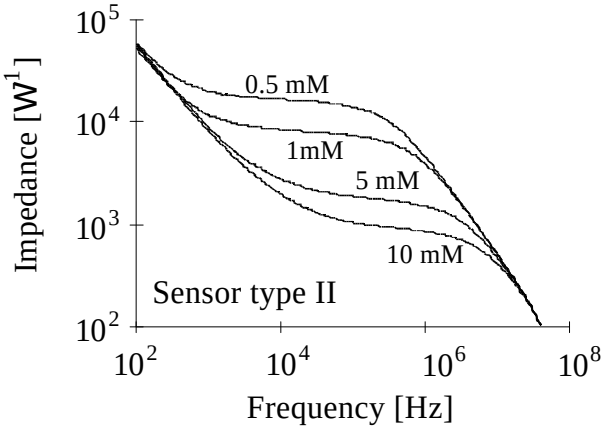

Figure 7: Measured impedance versus frequency of a structure of type II in KNO_3.

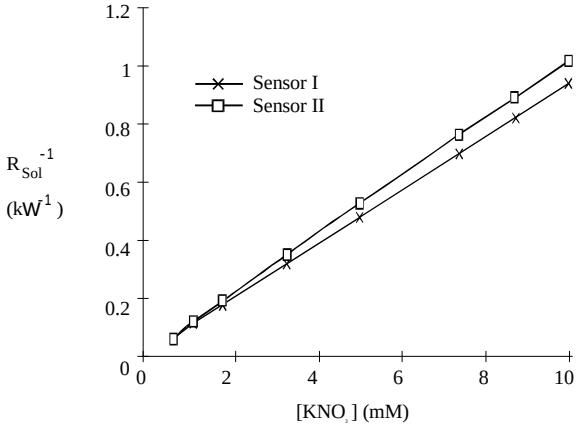

Figure 8: Measured calibration curve for conductivity measurement operation.

The electrolyte resistance R_{Sol} can be found from the impedance plot by taking the value of the impedance at the plateau. Taking into account that conductivity is proportional to the inverse of this resistance (according to equation 2), the admittance at the measured plateau ($1/R_{Sol}$) is plotted in figure 8. From the slope of this curve the cell constant can be calculated. This results in values of 1.35 and 1.28 cm^{-1} for structure I and II respectively.

4.3 Hydrogen peroxide concentration

The structure of figure 2 was used as an amperometric working electrode by connecting inputs A, B, C and D to the working electrode lead of an EG&G PAR 173 potentiostat. A two electrode set-up was used with a platinum 5´10 mm counter/reference electrode.
Figure 9 shows the recorded current responses on a potential sweep starting at 0 Volt and scanning with 500 mV per second to -1.2 Volt. Hydrogen peroxide concentrations of 25, 50 75 and 100 mM where tested directly after dilution from a 30% stock solution. A background electrolyte was used of 100 mM potassium nitrate was used to reduce the ohmic drop across the solution. Although the location of the peaks is unpredictable due to the unknown potential of the platinum counter electrode, the height of the peaks is directly proportional to the hydrogen peroxide concentration. Figure 10 can be used as a calibration curve for this type of measurement.

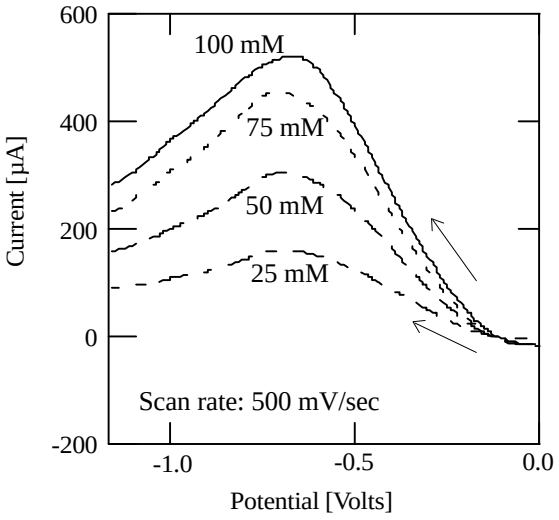

Figure 9: Experimental potential sweep amperometry results in hydrogen peroxide.

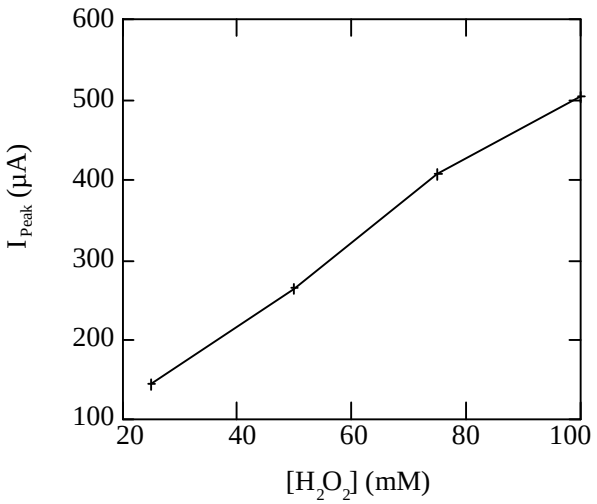

Figure 10: Calibration curve for amperometric detection operation of H_2O_2

4.4 Heating

After the thermo resistive paths were calibrated for temperature measurements as described before, the dissipated heat could be measured. This was done by applying a current to one branch (pads A and B), while measuring the resistance of another (pads C and D). With the given nominal resistances, a heating current of some tens of milli-amperes will result in a potential drop along the resistor in the order of volts. Because the structure is in contact with the electrolyte, this might result in electrochemical interferences. However, with an AC heater current this potential drop will not affect the electrolyte since it will largely be present over the electrode-electrolyte interface.

Figure 11 shows the transient response when heating with a sine wave of 1 kHz and an effective current of 35 mA. The 95% response time appears to be 8.9 seconds. Figure 12 shows the linear relation between the square of the applied current and the measured temperature. The increase in temperature was limited here by the sine wave generator which could not apply more then 35 mA.

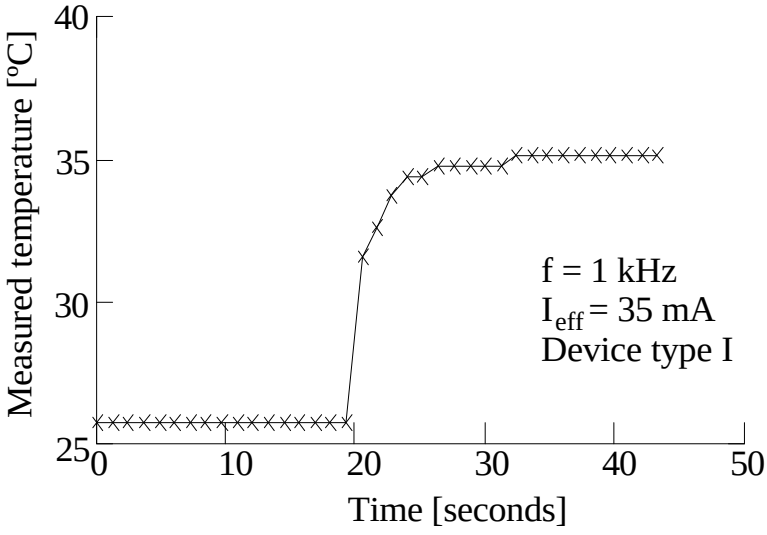

Figure 11: Measured transient response of a resistive branch while heating with another. Note, that heating started at approximately t = 19 sec.

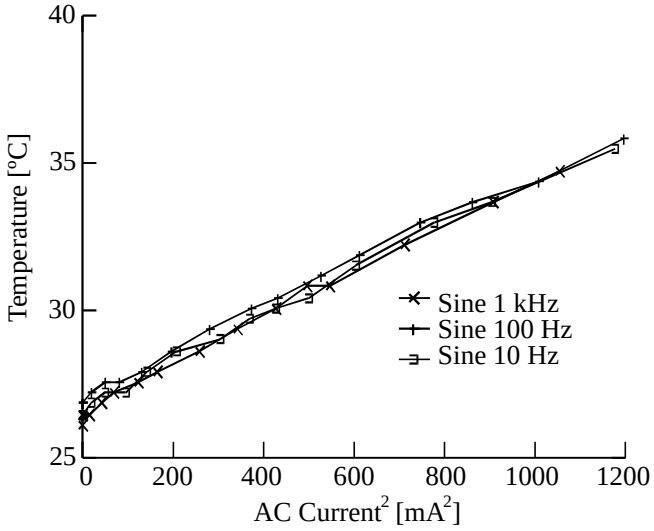

Figure 12: Measured calibration curve for the thermo resistive heating operation.

4.5 Control of pH gradient

As explained in section 3.5, the pH actuator operation was tested by doing a coulometric acid base titration. Therefore, the structure of figure 2 was used as a potentiometric working electrode by connecting inputs A, B, C and D to the working electrode lead of an EG&G PAR 173 potentiostat. A three electrode set-up was used with a platinum 5´10 mm counter electrode and a silver-silverchloride reference electrode.
The titration was carried out in a 0.10 M acetic acid (HAc) solution with 0.10 M potassium nitrate as a background electrolyte. Using an applied current of 100 µA, the observed potential behaved like represented in figure 13.

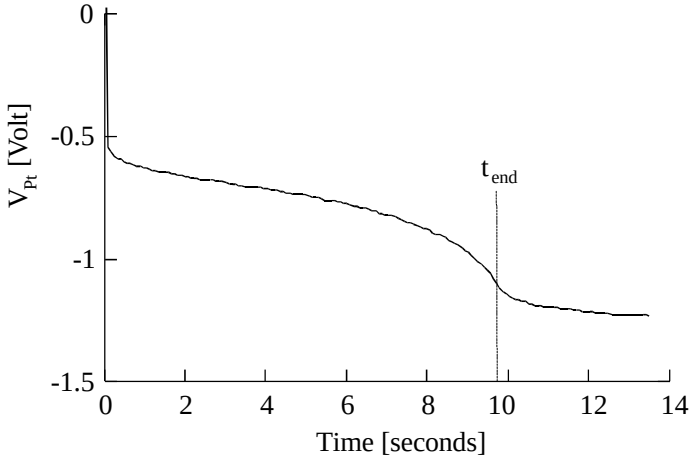

Figure 13: Chronopotentiogram of a coulometric titration in 0.10 M HAc using an actuator current of 100 µA.

The measured end point of the titration is 9.71 seconds which results in a measured HAc concentration of 0.109 M using a diffusion constant of $1.21 \cdot 10^{-9}$ m^2 sec^{-1} for HAc [6] and the electrode area size as given in table 1. As expected this value is almost equal to the prepared concentration.

5. Conclusions and future work

Using the proposed miniaturised multi purpose sensor-actuator structure, three parameters were successfully measured. Besides the three basic sensing operational modes, two actuator modes were performed. Together with the sensor modes this gives a real multi purpose integrated sensor-actuator device with which many local experiments can be performed in order to analyse a solution more completely than was possible using some particular single sensors. Having two actuator and three sensor operations, there will be six sensor-actuator combinations. By selecting a certain sensing mode while applying an actuator mode, a local "micro experiment" is carried out yielding new parameters. For instance, heating while measuring temperature gives information on the movement of the medium (a flow sensor). Another example is the generation of hydroxide ions while a potentiometric determination is done in order to do a coulometric acid to base titration. Actually, this was already used to verify the pH gradient control mode in section 0. The major aim of future research is to evaluate all possible combinations.
The three sensor operations and two actuator modes were obtained by connecting the structure to advanced laboratory equipment. In future a dedicated control box will be constructed which schedules these operational modes sequentially or simultaneously.

Acknowledgement

This research project is financially supported by Unilever.

References

[1] J. Janata and M. Josowicz, Chemical sensors, Analytical Chemistry 70, pages 179R - 208R, 1998.
[2] P. Jacobs, A. Varlan, W. Sansen, Design optimisation of planar electrolytic conductivity sensors, Medical & Biological Engineering & Computing, November 1995.
[3] David R. Lide, Handbook of chemistry and physics, 74th edition 1993-1994, CRC Press Inc.
[4] A.J. Bard and L.R. Faulkner, Electrochemical methods: fundamentals and applications, John Wiley & Sons, New York, 1980.
[5] Carslaw and Jaeger, Conduction of heat in solids, Clarendon Press, Oxford, 1959.
[6] W. Olthuis and P. Bergveld, Integrated coulometric sensor-actuator devices, Mikrochim. Acta 121, pages 191-223, 1995.

Biographies

Geert Langereis was born in Apeldoorn, the Netherlands, on April 11, 1970. He received the M.Sc. degree in electrical engineering from the University of Twente, Enschede, the Netherlands in 1994. During his study he achieved both a biomedical and an ergonomical endorsement. He is currently working on a Ph. D. project on integrated sensor arrays in the Biosensor Technology Group, part of the MESA Research Institute, of the University of Twente.

Wouter Olthuis was born in Apeldoorn, the Netherlands, on October 23, 1960. He received the M.Sc. degree in electrical engineering from the University of Twente, Enschede, the Netherlands in 1986, and the Ph.D. degree from the Biomedical Engineering Division of the Faculty of Electrical Engineering, University of Twente, in 1990. The subject of his dissertation was the use of Iridium oxide in ISFET-based coulometric sensor-actuator devices. Currently he is working as an Assistant Professor in the Biosensor Technology Group, part of the MESA Research Institute, of the University of Twente.

Piet Bergveld was born in Oosterwolde, The Netherlands, on January 26, 1940. He received the M.Sc. degree in electrical engineering from the University of Eindhoven, the Netherlands, in 1965 and the Ph.D. degree from the University of Twente, the Netherlands, in 1973. The subject of his dissertation was the development of ISFETs and related devices, the actual invention of the ISFET, since then also investigated by many international research groups of Universities as well as industry. Since 1965 he has been a member of the Biomedical Engineering Division of the Faculty of Electrical Engineering (University of Twente) and was in 1984 appointed as Full Professor in Biosensor Technology. He is one of the project leaders in the MESA Research Institute. His research subjects still concern the further development of ISFETs and biosensors based on ISFET technology as well as physical sensors for biomedical and environmental applications, resulting up to now in more than 250 papers. He recently was appointed as a member of the Royal Dutch Academy of Science.